

Grzegorz KŁOSOWSKI  
Tomasz RYMARCZYK  
Konrad KANIA  
Antoni ŚWIĆ  
Tomasz CIEPLAK

## MAINTENANCE OF INDUSTRIAL REACTORS SUPPORTED BY DEEP LEARNING DRIVEN ULTRASOUND TOMOGRAPHY

### EKSPLOATACJA REAKTORÓW PRZEMYSŁOWYCH ZE WSPOMAGANIEM TOMOGRAFII ULTRADŹWIĘKOWEJ I ALGORYTMÓW GŁĘBOKIEGO UCZENIA

*Monitoring of industrial processes is an important element ensuring the proper maintenance of equipment and high level of processes reliability. The presented research concerns the application of the deep learning method in the field of ultrasound tomography (UST). A novel algorithm that uses simultaneously multiple classification convolutional neural networks (CNNs) to generate monochrome 2D images was developed. In order to meet a compromise between the number of the networks and the number of all possible outcomes of a single network, it was proposed to divide the output image into 4-pixel clusters. Therefore, the number of required CNNs has been reduced fourfold and there are 16 distinct outcomes from single network. The new algorithm was first verified using simulation data and then tested on real data. The accuracy of image reconstruction exceeded 95%. The results obtained by using the new CNN clustered algorithm were compared with five popular machine learning algorithms: shallow Artificial Neural Network, Linear Support Vector Machine, Classification Tree, Medium k-Nearest Neighbor classification and Naive Bayes. Based on this comparison, it was found that the newly developed method of multiple convolutional neural networks (MCNN) generates the highest quality images.*

**Keywords:** *deep learning; inverse problem; ultrasound tomography; image reconstruction; process tomography.*

*Monitorowanie procesów przemysłowych jest ważnym elementem zapewniającym właściwą eksploatację urządzeń i wysoki poziom niezawodności procesów. Prezentowane badania dotyczą zastosowania metod głębokiego uczenia w obszarze eksploatacji zbiornikowych reaktorów przemysłowych. W procesach przemysłowych opartych na reakcjach chemicznych zachodzących wewnątrz procesowej tomografii ultradźwiękowej (UST). Opracowano nowatorski algorytm wykorzystujący jednocześnie wiele klasyfikacyjnych spłotowych sieci neuronowych (CNN) do generowania monochromatycznych obrazów 2D. Aby osiągnąć kompromis między liczbą sieci a liczbą wszystkich możliwych wyników pojedynczej sieci, zaproponowano podział obrazu wyjściowego na klastry 4-pikselowe. W związku z tym liczba wymaganych CNN została czterokrotnie zmniejszona i istnieje 16 różnych wyników z jednej sieci. Nowy algorytm został najpierw zweryfikowany przy użyciu danych symulacyjnych, a następnie przetestowany na danych rzeczywistych. Dokładność rekonstrukcji obrazu przekroczyła 95%. Wyniki uzyskane przy użyciu nowego algorytmu klastrowego CNN zostały porównane z pięcioma popularnymi algorytmami uczenia maszynowego: płytką sztuczną siecią neuronową, maszyną liniowego wektora wsparcia, drzewem klasyfikacji, klasyfikacją średniego k-najbliższego sąsiada i naiwnym Bayesem. Na podstawie tego porównania stwierdzono, że nowo opracowana metoda wielu spłotowych sieci neuronowych (MCNN) generuje obrazy o najwyższej jakości.*

**Słowa kluczowe:** *uczenie głębokie; problem odwrotny; tomografia ultradźwiękowa; rekonstrukcja obrazu; tomografia procesowa.*

## 1. Introduction

### 1.1. Tank chemical reactors

The basic device for the implementation of the batch processes are tank reactors. Batch processes are widely used in many branches of economy e.g. food, chemistry, pharmacy, semiconductors, biogas plants and so on. Due to the time-varying, non-linear and uneven nature of this process, it is very difficult to determine the exact mathematical model of these processes, which necessitates their monitoring. For this reason, to ensure a high level of reliability and trouble-free

maintenance of tank reactors it is necessary to effectively monitor the processes taking place inside them.

A tank chemical reactor is, in the simplest sense, a vessel adapted to carry out a specific chemical reaction in it. On an industrial scale, the construction of a reactor and the parameters of its process should ensure optimal economic results. Chemical reactors and the processes taking place in them are usually an essential element of a technological process aimed at producing a specific chemical product. Any other processes in such a sequence should be assigned a rather auxiliary role, consisting either in preparatory activities or in separating the products of the reaction and separating from them the component, the obtaining of which is the aim of production operations. Produc-

tion and economic results usually depend on the correct operation of a chemical reactor. The chemical process occurring in the reactor overlaps, to varying degrees and in different proportions, the processes of mass, momentum and heat transfer. This usually gives a very complicated picture of the total process. The description of these total complex processes can often be simplified if one of the mentioned processes plays a dominant role in it and the others can be omitted. The most often such a dominant elementary process is the transport of mass or energy. Effective monitoring of these types of processes requires non-invasive methods that include tomography.

In the reactor classification prepared according to the type of reagent cluster state, we distinguish two basic reactor groups - homogeneous and heterogeneous. In heterogeneous reactors, gas and solids, gas and liquid, solids and liquids can react with each other. The presented studies concern the monitoring of industrial two-phase processes of solids and liquids (crystallization) and liquids and gases (detection of gas bubbles in liquids or suspensions).

A specific type of chemical reactors are bioreactors. Bioreactors comply with the same rules as chemical reactors. The difference, however, lies in the complexity of the system which is a living organism. Biological reactions are more sensitive and less stable, and therefore require more attention to process control and analysis of more factors than chemical reactions. In order to ensure the proper operation of bioreactors, it is necessary to use an effective method of monitoring industrial processes. In this context, the issues of monitoring biological processes deserve attention [1,24,34].

To rationally control the maintenance processes of technical facilities, including reactors, it is necessary to know about the state of these objects. To this end, various monitoring methods are used. Monitoring allows you to solve important maintenance problems, which include maximizing reliability and process diagnostics [40]. Tomography is a cheap and non-invasive method of monitoring, but in industry, this method does not always allow obtaining high resolution images. For this reason, research is needed that will lead to the method of industrial tomography, which will guarantee high-resolution cross-sectional images of the examined objects. This article refers to a new method of ultrasonic tomography using deep learning algorithms [19].

## 1.2. Tomographic methods and algorithms

Tomography is used in the areas where obtaining good image quality involves the use of a non-invasive monitoring method [9]. There are many types of tomographic methods, including: computed tomography (CT) [3,29], radio tomographic imaging (RTI) [5], electrical impedance tomography (EIT) [30,31], electrical capacitance tomography (ECT) [4,16,17,22,42] or ultrasound tomography (UST) [45].

UST enables non-invasive visualization of the interior of the tested object based on measurements of the time of sound propagation between different points on the perimeter of the tank. The presence of inclusions in the object changes the time of fly of sound waves. On this basis, the cross-sectional image of the tested tank can be reproduced. The main problem of UST is the difficulty of building a physical model that would be able to take into account the full complexity of acoustic phenomena occurring in a relatively small space [8]. This causes problems in implementing classic tomographic methods. This work is our first attempt to verify the hypothesis that a properly constructed neural network is able to solve the inverse problem in ultrasound tomography. Positive results obtained in this work give hope that some problems related to modeling can be bypassed by means of convolutional neural networks (CNN) [38].

Considering the number and frequency of publishing new scientific studies on innovative industrial solutions - the UST method is relatively less widespread. In the field of industrial applications, most innovations are created in the areas of electrical impedance tomog-

raphy [13,32], electrical capacitance tomography (ECT) [27,28,35] and magnetic resonance imaging [23,15]. Progress is made both in the field of hardware (sensors, computer distributed systems) and in the field of reconstruction algorithms for tomographic images. The classic methods of solving the inverse problem in the tomography include Gauss Newton's (GN) method. Compared to machine learning methods, the GN method is more universal, which means that it can be used in commercial tomographs on a wider range of applications. When it comes to problems for which machine learning algorithms can be trained, the GN method is rather less precise and increasing precision of GN method requires the usage of iterative methods, which significantly slows the algorithm.

Among the statistical methods of machine learning, the following methods have been successfully applied in the reconstruction of tomographic images, especially in electrical tomography: elastic net, lasso (least absolute shrinkage and selection operator), least-angle regression (LARS) [6], k-nearest neighbors (KNN), naive Bayes, multivariate adaptive regression splines (MARS), classification tree, support vector machine (SVM), gradient boosting machine (GBM) [21], principal component or partial least square regression [22]. There is a general trend that the importance of predictive algorithms is growing in industrial applications [41,12,14,20,10].

Due to the specific conditions of the functioning of industrial systems, the use of electrical tomography is not always possible. In situations where the tested object cannot be completely isolated from the influence of other sources of electric current or when the tested environment is dielectric, ultrasound tomography (UST) can be used. There is evidence in the literature of the effective use of UST in medicine which may indicate the existence of unused potential of ultrasound process tomography [36].

Hao et al. localized the fetal abdominal standard plane from ultrasound recordings using CNN [7]. In that case, the accuracy of the system reached 90%. Zhang et al. proposed a diagnosis system based on the two-layer CNN architecture for the classification of breast tumors [43]. The accuracy of the system they developed was 93.4%. Ma et al. classified thyroid nodules based on ultrasound, using two CNNs simultaneously. The average classification efficiency was 83.02% [21]. In other medical studies, Arevalo et al. classified changes in breast cancer from hand-segmented mammography films using CNN. They managed to achieve an accuracy of 82% [2].

The above and other examples of successful combination of UST and CNN in medical applications have given rise to targeted research on effective technics for reconstructing tomography images based on the measurements of the time-of-flight of the ultrasonic waves in an industrial tank. The non-destructive UST method supported by deep learning algorithms is suitable for monitoring industrial processes occurring not only inside closed reactors but also flow processes inside complicated pipe systems.

## 1.3. Convolutional neural networks

CNN has in recent years become the leading topic of technical progress in many areas [37]. Due to the high ability to recognize specific features visible on CNN images, they are often used in various classification problems [26,6]. Other areas of CNN application include image classification [25], video analysis, natural language processing, city monitoring, industrial cameras and all kinds of devices providing images made with ordinary photographic techniques [44]. Creating images obtained by resolving the inverse problem, such as tomographic images, is a relatively new area of application for CNN and is therefore difficult [18,11].

CNNs are good in mapping complex nonlinear functions. For this reason, the number of attempts to use deep learning algorithm for image reconstruction in EIT/ERT (electrical impedance tomography/ electrical resistance tomography) is increasing [39].

Attempts are also made to create hybrid methods, an example of which is a real-time reconstruction algorithm that produces high-quality sharp EIT absolute images by combining the D-bar algorithm with subsequent CNN processing [19].

1.4. Research objective and novelties

The main goal of the research presented in this article was to develop a new algorithm capable of reconstructing monochrome (binary) 2D images of ultrasound tomography, regardless of the size, shape, location or number of inclusions hidden in the examined object.

High accuracy of imaging is achieved thanks to splitting the outputs for multiple CNNs. The higher speed of the algorithm is reached thanks to the use of 4-pixel clusters approach. Instead of training CNN networks for all 1024 pixels, there are only 256 networks to train, one for each cluster. As a result, we get a 4-fold increase in the speed of the algorithm, preserving reasonably small number of possible outcomes of the CNNs.

Fig. 1a shows the scheme of the algorithm based on the structure of an ordinary CNN with 496 inputs and 1024 binary outputs (0, 1). In Fig. 1b, for comparison, proposed multiple CNN scheme is shown. Each of the 256 CNNs generates a numerical classifier {1..16} at the output, which is the cluster identifier. Then, each cluster is converted to a 4-pixel monochrome pattern with dimensions of 2x2 (Table 1).

This article consists of 4 sections. Section 1 presents the state of art regarding tomographic methods and algorithms used in the reconstruction of tomographic images. Specific examples of UST applications combined with deep learning are presented. Section 2 contains a detailed description of the test stand, the data used, the multiple CNN algorithm, as well as information on the learning process. Section 3 presents examples of reconstructions obtained by using the

multiple CNN method. In addition, the quality of this method was compared with 5 other classical machine learning algorithms.

2. Hardware, Algorithms and Methods

2.1. The hardware

The research used a tomographic system developed by the authors of this publication. Fig. 2a shows the mesh of lines indicating measurements of the speed of the sound wave. The densities of the lines at the periphery of the tank cross section are determined by 32 transducers. Fig. 2b demonstrates the test stand. Based on measurements from this stand, effective algorithm for generating simulation data was developed.

The tomograph is built on the STM32F103VCT6 processor (Fig. 3a) which is responsible for the managing of a measurement sequence and setting transducers in the transmitting or receiving mode. Measurement data acquisition system cooperates with dedicated transducers, as shown in Fig. 3b. Measurements data can be transmitted to the PC in real time (Fig. 3c).

The transducers performs measurements using one piezoelectric unit using the absorption method. The transducer can work both as a transmitter and an ultrasonic wave receiver. The transducer has an integrated signal processing system and a microcontroller with a built-in A/C converter. By using a programmable digital potentiometer, the gain of the received signal can be regulated. The PCB transducer also provides the option of filtering out the signal using an active filter. A small diode is used to signal the operating status of the device.

Control and reading of measurements made by the transducer is carried out via the CAN 2.0A bus. Due to the special design, the

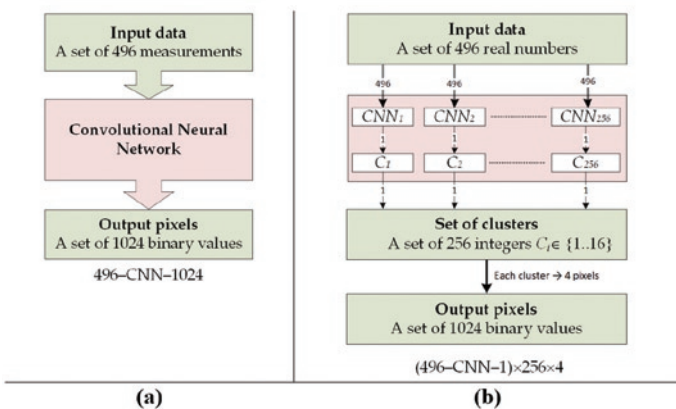


Fig. 1. Comparison of algorithms for methods CNN (a) and MCNN (b)

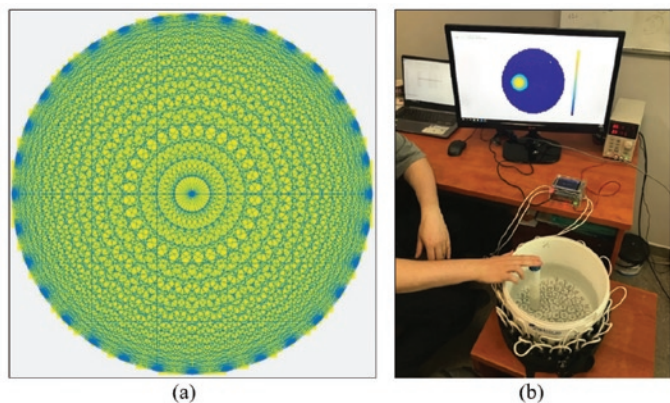


Fig. 2. (a) - A mesh of measurements carried out by 32 transducers arranged around the tank; (b) - View of the test stand [33]

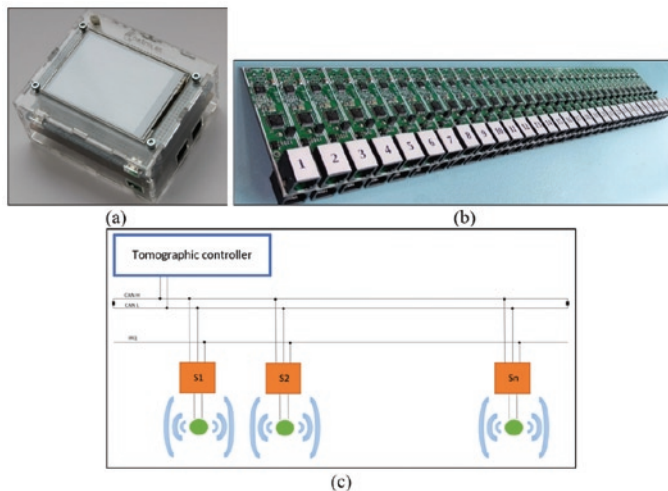


Fig. 3. (a) - Controller running on the STM32F103VCT6 processor; (b) - View of composite 32 PCBs of ultrasound transducers; (c) - Block diagram of the system

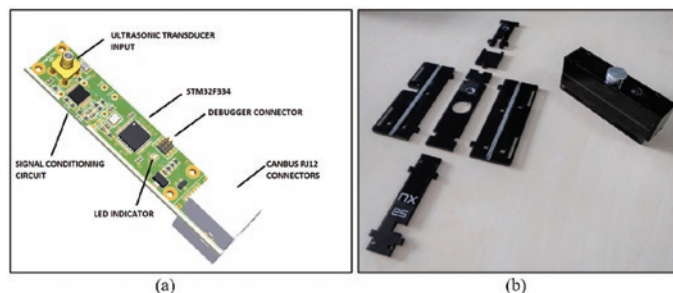


Fig. 4. Design of the active measuring transducer: (a) motherboard; (b) assembly

transducers can be installed in close proximity to each other. RJ-12 cables were used to make the communication buses and to provide power supply. Each transducer was divided into two parts - digital and analog. The task of the digital part is to send the measurement results to the tomographic controller. The analog part of the transducer was adapted to work with a 40 kHz piezoelectric unit (Fig. 4a and 4b).

2.2. Algorithms and Methods

In order to solve the inverse problem, classification convolutional neural networks (CNNs) were used. During the research, it turned out that a single convolution network powered by 496 measurements and generating 1024 binary elements learns very long and the obtained results are not good enough. The novel element of the presented solution is to use CNN to classify 4-pixel clusters.

During a single measurement series, each of the transducers acts as an emitter, while the other transducers receive ultrasound signals at that time. When the number of transducers is 32, the number of measurements can be calculated as  $(32^2 - 32)$ . Since the time the sound wave needs to travel from A to B is the same as from B to A, the number of measurements  $M$  can be reduced by half. Hence, we get the relationship (1).

$$M = \frac{n^2 - n}{2} \tag{1}$$

where  $n$  is the number of transducers.

So the measurement vector establishing the MCNN input set that consists of 496 measurements. Each measurement means the so-called sound wave flight time between a specific pair of transducers. To ensure correct measurements, a reference measurement in an inclusion-free environment should be performed before actual measurements can begin. This is to determine the background values. Inclusions distort measured times, so that images can appear on the basis of contrast to the background. Based on different measurements of times, the locations and size of inclusions are determined.

An industrial tank filled with tap water played the role of the examined object. Various objects were immersed in water, followed by ultrasonic measurements. Thanks to the knowledge of the location and dimensions of the immersed objects, as well as the knowledge of the number of all inclusions, it was possible to develop a simulation algorithm that generated 20,000 learning cases. Fig. 5 shows a simulation example of generating one of 20,000 measurement cases.

The left side of the drawing illustrates the exemplary cross-section of the tank interior with visible inclusions. The right side is a graph of 496 measurements (horizontal axis), along with the corresponding transition times of ultrasound waves between pairs of transducers. In the simulation algorithm, Gaussian noise has been implemented with a distinct level for each measurement in the frame. The level of the noise was determined by the standard deviation set to 5% of the value of each measurement. The algorithm based on convolutional neural networks was developed using the Deep Learning Toolbox of Matlab.

As mentioned before, each learning case consisted of 496 input measurements and one monochrome output image with a resolution of  $32 \times 32$ . The number of measurements is the result

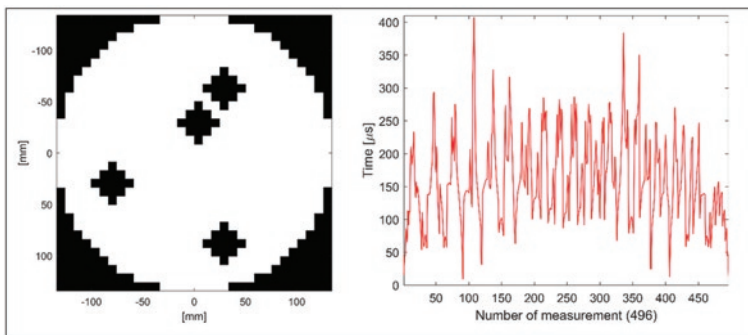


Fig. 5. A measuring case generated with the simulation method with a graph showing the times of sound waves moving between transducers

of using 32 transducers. The full matrix of measurements counts 992 ( $32 \times 31$ ) measurements, of which half of the measurements concern the same transducers. Because the sound wave moves at the same speed regardless of the direction ( $v_{1-2} = v_{2-1}$ ), the measurement matrix tend to be symmetrical one. Therefore by averaging symmetrical measurements we obtain 496 inputs for one measurement cycle. The  $32 \times 32$  monochrome image can be represented by a 1024-point vector with binary values 0 or 1. The method of converting pixels into clusters is shown in Fig. 6.

The Fig. 6 distinguishes three sample clusters with identifiers: 1, 51 and 137, as well as the method of changing pixels into the array of clusters. For example, cluster [1] contains pixels [1, 2; 33, 34]. After transforming pixels  $\rightarrow$  clusters, a matrix of 1024 pixels with dimensions of  $32 \times 32$  is reduced to a  $16 \times 16$  matrix composed of 256 clusters.

Formally, a distinct block of four pixels from a full image can be expressed as (2):

$$B_n = \begin{bmatrix} x_n & x_{n+32} \\ x_{n+1} & x_{n+33} \end{bmatrix} \tag{2}$$

assuming that  $n$  is an odd number. This block is transformed into a cluster with a number  $k(B_n)$  (3):

$$k(B_n) = \frac{1}{2} \left( (n-1) \% 32 + 16 \frac{n-1}{32} \right) + 1 \tag{3}$$

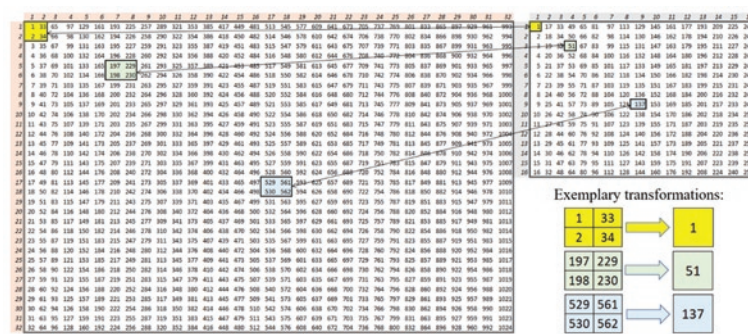


Fig. 6. The way to convert 1024 pixels into 256 clusters

Table 1. Pattern indexes  $p_i = \{1, 2, \dots, 16\}$

$P_i$	1	2	3	4	5	6	7	8	9	10	11	12	13	14	15	16
pattern																

where  $a \% b$  means the remainder of division  $a$  by  $b$  for  $a = (n - 1)$ ,  $b = 32$  and  $\lfloor \cdot \rfloor$  is the floor function.

Since the clusters have dimensions of  $2 \times 2$  that means that there are  $2^4 = 16$  combinations of binary patterns for each cluster. The possible binary patterns of clusters are presented in Table 1.

Transforming pixels into clusters reduces number of output variables to 256. We were decided to train 256 separate CNNs, each of which generated a value from 1 to 16, corresponding to the given cluster pattern. So in this case we are talking about multiple convolutional neural networks (MCNNs), where each of the distinct CNN solves the classification problem. Table 2 shows the structure of the convolutional neural network. Each of 256 CNNs has the same structure including 15 layers.

CNNs work in the same way as typical convolutional networks used for image recognition with the input vector of 496 measurements converted into a  $31 \times 16$  matrix.

Table 2. The structure of the convolutional neural network

ID	Name	Type	Activations	Learnables
1	imageinput 31x16x1 images with 'zerocenter' normalization	Image Input	31x16x1	-
2	conv_1 96 3x3x1 convolutions with stride [1 1] and padding 'same'	Convolution	31x16x96	Weights 3x3x1x96 Bias 1x1x96
3	batchnorm_1 Batch normalization with 96 channels	Batch Normalization	31x16x96	Offset 1x1x96 Scale 1x1x96
4	relu_1 ReLU	ReLU	31x16x96	-
5	avgpool_1 2x2 average pooling with stride [1 1] and padding [0 0 0 0]	Average Pooling	30x15x96	-
6	conv_2 16 3x3x6 convolutions with stride [1 1] and padding 'same'	Convolution	30x15x16	Weights 3x3x6x16 Bias 1x1x16
7	batchnorm_2 Batch normalization with 16 channels	Batch Normalization	30x15x16	Offset 1x1x16 Scale 1x1x16
8	relu_2 ReLU	ReLU	30x15x16	-
9	avgpool_2 2x2 average pooling with stride [1 1] and padding [0 0 0 0]	Average Pooling	29x14x16	-
10	conv_3 16 3x3x16 convolutions with stride [1 1] and padding 'same'	Convolution	29x14x16	Weights 3x3x16x16 Bias 1x1x16
11	batchnorm_3 Batch normalization with 16 channels	Batch Normalization	29x14x16	Offset 1x1x16 Scale 1x1x16
12	relu_3 ReLU	ReLU	29x14x16	-
13	fc 16 fully connected layer	Fully Connected	1x1x16	Weights 16x6496 Bias 16x1
14	softmax softmax	Softmax	1x1x16	-
15	classoutput crossentropyx	Classification Output	-	-

Fig. 7 shows the course of training the CNN, which task was to classify the pattern for cluster No. 137. It was noted that the cluster No. 137 is a case that makes reconstruction more difficult than other clusters - hence the choice. The mini-batch size for CNN was set to 64. Validation frequency was 30 and number of epochs was 10.

Validation accuracy equals 95.9%. Accuracy is calculated as the ratio of accurately guessed classifiers to all validation cases. Maximum iterations limit was 2960. Training finished because it reached final iteration, not due to the lack of a decrease of the validation error in the next 6 iterations.

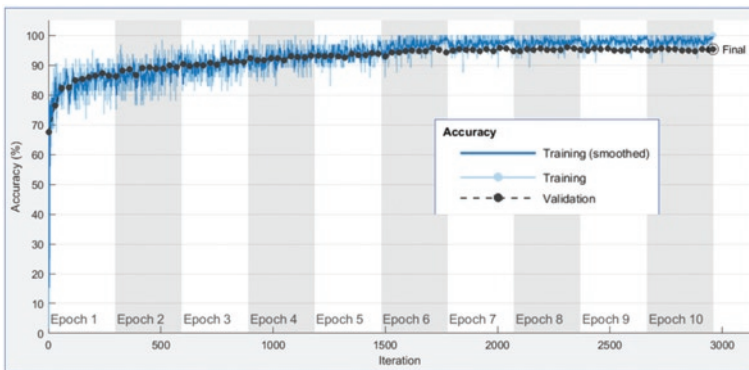


Fig. 7. Training progress through accuracy for cluster No. 137

Fig. 6 corresponds with Fig. 8. It shows training progress through loss indicator for cluster No. 137. The Validation loss is calculated as the ratio of incorrectly guessed classifiers to all validation cases.

By analyzing the shapes of the graphs presented in Fig. 7 and 8 we can conclude that the CNN learning process for the cluster No. 137 proceeded correctly. The initial, large increase in accuracy and the subsequent lack of fluctuations indicate the lack of overfitting. Also, the validation loss at 0.1398 allows us to conclude that CNN has a high generalization capability.

The above results are confirmed in Table 3, where selected itera-

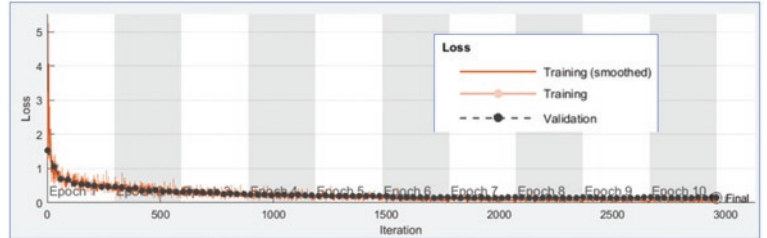


Fig. 8. Training progress through loss indicator for cluster No. 137

tions, from the CNN learning process for the cluster No. 137, are presented. Base Learning Rate is variable and decreases with subsequent epochs. The algorithm updates the learning speed by reducing the Learning Rate, multiplying it by a specific fractional learn-rate drop factor within a certain number of epochs.

Table 3. Training CNN for cluster No. 137 on single GPU

Epoch	Iteration	Time Elapsed	Mini-batch	Validation	(Mini-batch)	Validation	Base Learning
		(hh:mm:ss)	Accuracy	Accuracy	Loss	Loss	Rate
1	1	00:00:00	17.15%	76.20%	2.4260	1.2312	0.0100
1	270	00:00:10	87.50%	87.50%	0.5279	0.3940	0.0100
1	300	00:00:11	89.06%	89.10%	0.4350	0.3766	0.0100
2	570	00:00:21	85.94%	91.50%	0.2722	0.2509	0.0100
3	600	00:00:22	90.63%	91.90%	0.2496	0.2520	0.0100
3	870	00:00:32	95.31%	92.90%	0.2569	0.2173	0.0100
4	900	00:00:33	98.44%	92.80%	0.1025	0.2224	0.0100
4	1170	00:00:43	92.19%	93.80%	0.1765	0.1952	0.0100
5	1200	00:00:44	96.88%	94.30%	0.1214	0.1941	0.0100
5	1470	00:00:54	100.00%	93.80%	0.0361	0.1822	0.0100
6	1500	00:00:55	100.00%	94.10%	0.0869	0.2011	0.0020
6	1770	00:01:05	98.44%	95.40%	0.0371	0.1524	0.0020
7	1800	00:01:06	98.44%	95.60%	0.0862	0.1494	0.0020
7	2070	00:01:16	98.88%	95.90%	0.0855	0.1398	0.0020
8	2350	00:01:27	98.44%	95.90%	0.0971	0.1398	0.0020
10	2960	00:01:51	96.88%	95.50%	0.0855	0.1398	0.0020

### 3. Results and discussion

#### 3.1. Reconstructions with simulation data

Fig. 9 presents 5 cases of reconstruction, made by applying our algorithm on simulation data for the ultrasound tomography. In order to make an objective assessment of the quality of the reconstruction, the accuracy indicator was used (4):

$$Accuracy = \frac{N_c}{N} \cdot 100\% \quad (4)$$

where:  $N_c$  – number of pixels reconstructed correctly,  $N$  – total number of pixels.

Individual cases in Fig. 9 were sorted according to the number of inclusions. The first case concerns a single, large inclusions. Its accuracy is the highest and amounts to 99.32%. With the exception of samples 3 and 4, one can see a regularity that the more inclusions, the worse the accuracy of the mappings. This is a typical phenomenon in tomography, which can be observed not only in relation to UST, but in EIT and ECT as well.

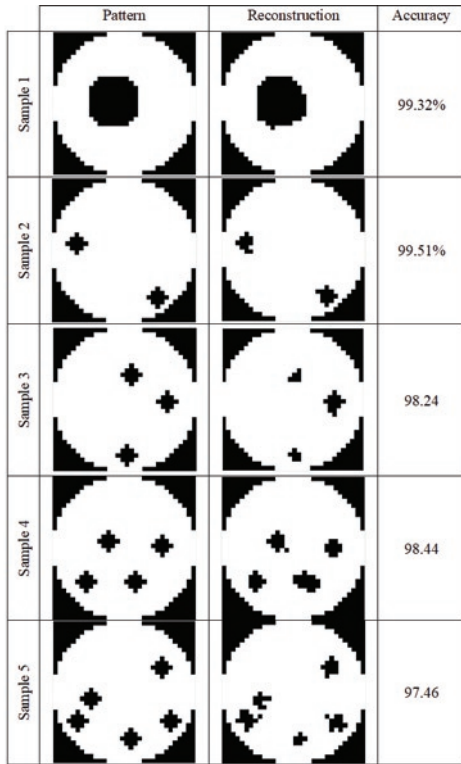


Fig. 9. Simulated reconstructions using MCNN

The general observation of the reconstructed samples shows that in all cases MCNN correctly reflects the size and location of the inclusions. Slightly more difficult are the cases of reconstruction many small objects. Sample 5 in Fig. 9 shows that despite some imperfections, one can still correctly determine both the location and size of the objects hidden in the tank.

Table 4 presents a comparison of the results of a single cluster (No. 137) reconstruction. Because the comparison was for a single cluster, not for the whole image, there was no need to use multiple CNN or multiple ANN.

All six methods listed in Table 4 have 496 measurements at the input, and at the output a classifier generating the numbers  $p_i = \{1, 2, \dots, 16\}$ . Cluster 137 is located in the central part of the observation field, which means that it is remote from all transducers. In the case of using CNN, the reconstruction accuracy of the cluster No. 137 is about 2.7% lower than the average accuracy of all reconstructed images listed in Fig. 9, hence the classification for that particular cluster seems to be slightly more difficult than for others. For comparative reconstruction

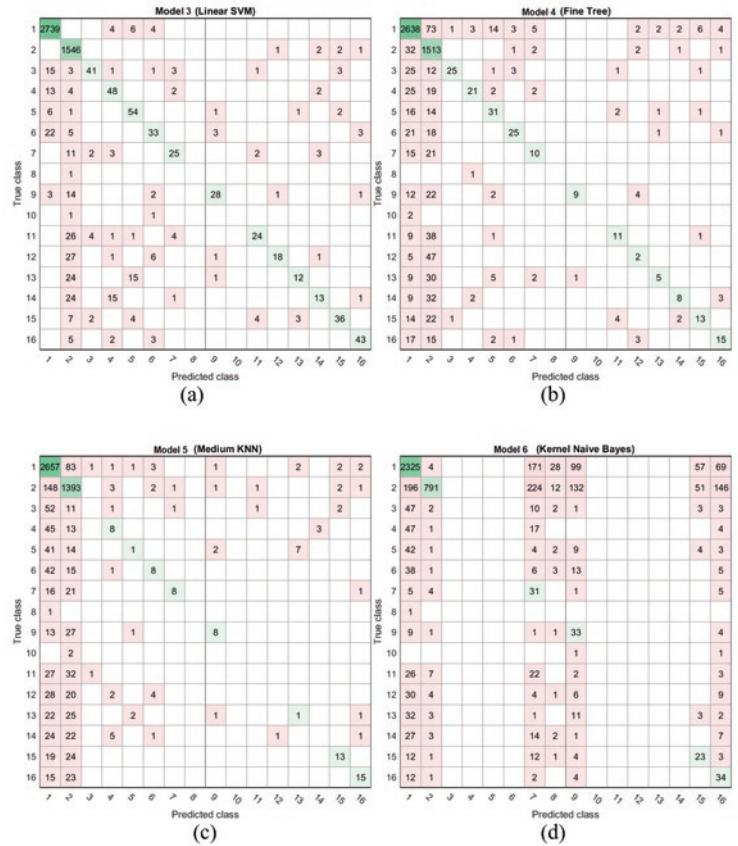


Fig. 11. Confusion matrices for: (a) SVM, (b) Fine Tree, (c) KNN, (d) Naive Bayes

of the cluster No. 137, the following classification techniques belonging to the group of machine learning methods were used: Convolutional Neural Network (CNN), Artificial Neural Network (ANN), Linear Support Vector Machine (LSVM), Classification Tree, Medium k-Nearest Neighbor classification (KNN) and Naive Bayes.

Fig. 10 shows confusion matrices of the cluster No. 137 for two types of neural network: deep CNN (a) and shallow ANN (b) (Table 4, ID 1-2). Fig. 11 shows confusion matrices for four statistical machine learning methods (Table 4, ID 3-6). The comparison of the accuracy indicator showed that the method based on CNN algorithms is the most exact.

Cases correctly reconstructed are marked in green. They are located along the diagonal of the matrix. The number of validation cases used to test accuracy was 4999.

Fig. 10 and 11 should be analyzed in relation to Table 1. The most accurate reconstruction concerned cluster No. 1 ( $p_i=1$  in Table 1).

It is a cluster without inclusions, completely white. This cluster occurs most often at any reconstruction because it depicts the background. Cluster No. 2 is the second most accurate classification ( $p_i=2$  in Table 1). This cluster contains one black pixel in the lower left corner of the 4-pixel area. This cluster can be used for reconstruction of small inclusions, or for imaging the edges of larger inclusions. It can be seen that, for the rest of the cluster, the CNN confusion matrix has

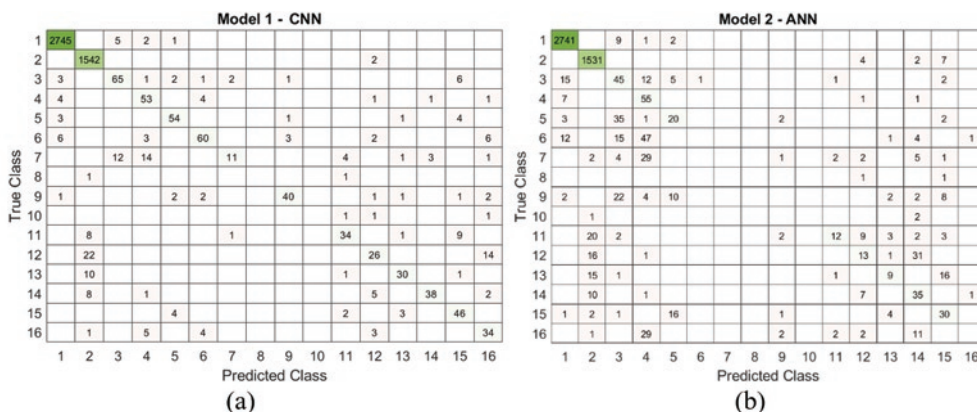


Fig. 10. Confusion matrices for: (a) – deep CNN, (b) – shallow ANN

the most correct hits, as evidenced by the high numbers along the diagonal (Fig. 10a).

Analyzing the results of classical confusion matrices, it should be taken into account that erroneous cases do not have to mean a total mistake in the means of quality of full image. For example two distinct patterns of clusters can differ only by one pixel, thus the whole image can still be reconstructed relatively correctly despite the mistake in classification.

### 3.2. Reconstructions with real data

Fig. 12 shows the test stand that was used to verify the MCNN algorithm based on real measurements. The measurements obtained from this setup were processed using MCNN trained on the simulation generated data. An adjustable frame was mounted on top of the bucket filled with tap water, allowing variable arrangement of vertical air-filled plastic tubes.

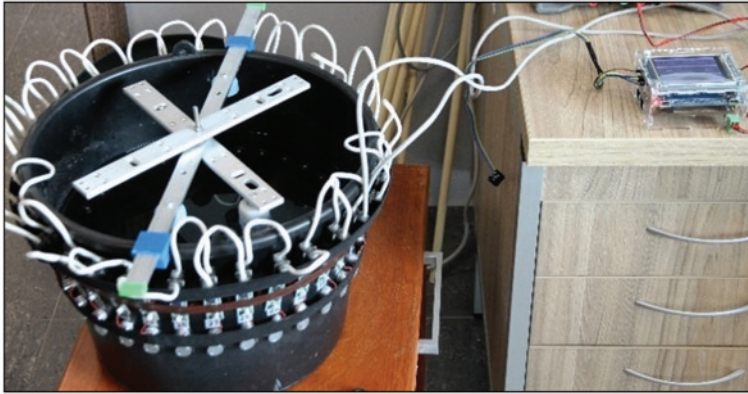


Fig. 12. Stand for collecting real data

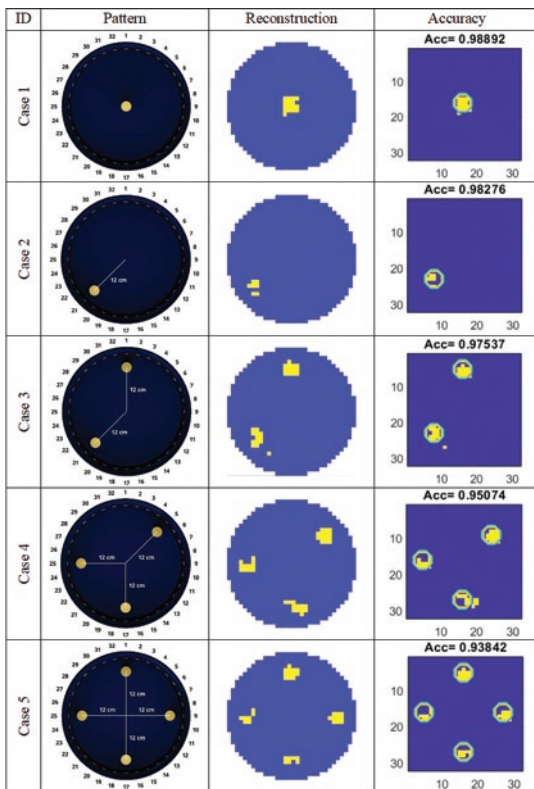


Fig. 13. Real data reconstruction using MCNN

Fig. 13 presents the results of reconstructions based on real measurements. Five cases were tested, which involved a varying number of objects immersed in water. For real reconstructions, reference images were developed based on geometric measurements.

Then the pattern images were applied to a 32×32 pixel matrix. In this way, accuracy was estimated based on relationship (4). Case 1 includes a single centrally located object equidistant from all 32 transducers. The reconstruction of this case is clear. The object has been correctly located, but its shape and dimensions are not reflected with high accuracy. In the tomographic image, the object has a larger diameter and its shape is not rounded.

Case 2 concerned a single object located close to the tank wall. Also in this case the position of the inclusions has been correctly illustrated, but the shape and dimensions are not perfect. In addition, the image of the object is heterogeneous. In fact, these are 2 objects located close to each other. This can be a problem during identifying the real number of inclusions.

Case 3 shows the reconstruction of two objects spaced apart. As in previous cases, the complaints concern the shape and size of reconstructed inclusions. In addition, one of the objects is represented as two separate objects that are close together, one of which is much larger than the other.

Cases 4 and 5 show reconstructions of 3 and 4 inclusions located near the walls of the tank, respectively. Assumptions from the observations are similar to those in previous cases. It is worth noting, however, that although the shapes and dimensions of the objects are not properly reconstructed, their location is determined relatively precisely and the reconstructed image is actually noise free. Based on the conducted experiments, it seems that the UST system works similarly regardless of the number of inclusions and irrespectively from the distance of hidden objects from the transducers.

## 4. Discussion

Because UST is a method rarely used in process tomography, it is reasonable to ask about the reasons for this. The answer is undoubtedly complex, but the main reasons are two.

The first reason is due to the difficulties in developing the appropriate physical model of sound's interaction [8]. The second reason is the imperfections of data processing algorithms. This work focuses on algorithms, although the UST tomograph used was designed and made by electronic engineers in Netrix SA laboratories. The developed hardware system proved to be good enough to provide sufficient quality data for efficient processing by the deep learning and training algorithm of a multi-convolutional neural network (MCNN) system. The developed method is a new proposal in the field of tomographic algorithms, and although it cannot be said that its use will always outweigh the effectiveness of other known methods, in all tested cases the MCNN algorithm proved to be the most effective.

Tracking the progress of research on algorithms, it can be seen that the unequivocal indication of one method that definitely outweighs the other methods of imaging efficiency in each case is impossible. Reviewing the research results presented by scientists, it can be stated that they depend on specific restrictions related mainly to the details of the research object. It is also known that for the algorithm to work properly, measurements must provide data on sizes and formats closely tailored to given requirements. This fact is the basic barrier hindering the construction of universal tomographs, suitable for a wide range of applications.

In these studies, experiments were conducted using a bucket of water in which plastic pipes were immersed. Simulation algorithms were validated based on the data obtained from measurements at the test stand (Fig. 2b). Thanks to simulation cases, including both precise reference images and their corresponding measurements, it was possible to

compare the effectiveness of several selected algorithms (CNN, ANN, LSVM, Classification Tree, KNN and Naive Bayes). The evaluation criterion was an objective indicator - Accuracy.

In addition to simulation tests, reconstructions of UST images were also made based on real data captured directly from the test stand. Due to the lack of precise reference images, a quantitative assessment of these cases was not possible. On the other hand, it was possible to visually compare the reconstruction with the arrangement diagrams of the inclusions in the individual cases studied. It turned out that despite the expected noise resulting from the presence of many unsteady factors accompanying processes carried out in complex electronic systems, the obtained reconstructions are legible and basically correctly reflect the positions of the inclusions relative to the examined cross-section. This is particularly important taking under consideration the binary specificity of imaging. The binary nature of imaging means that every error is visible in the image as an incorrectly displayed pixel what is a relevant issue due to small resolution of the image.

The limitation of MCNN may be a relatively low reconstruction speed. Although the speed of calculations depends on many factors, the need for a large number of separately working CNNs means that the presented method may not be used in flow systems or systems with high dynamics of change inside the tested tank. Therefore, potential areas of application for UST systems with MCNN algorithms relate to static 2-phase systems, e.g. tanks and reactors with liquid-solid phases, can be limited.

The advantage of MCNN is the ability to properly reconstruct the inclusion position and resistance to noise. Comparing the reconstructed images based on simulation and real data, it can be concluded that the algorithm effectively deals with noise. This is undoubtedly strength of MCNN especially due to the fact that the neural networks was trained on simulation data which are much more easier to collect, in the amount necessary for training process, than the real measurement data.

## 5. Conclusions

The article presents a new algorithmic method of deep learning, enabling accurate image reconstruction using ultrasound tomography (UST). Known and currently used methods of monitoring tank reactors are still burdened with problems resulting in a relatively low resolution of reconstructed images, hence it was necessary to take up the analyzed subject. The presented tomographic method contributes to improving the diagnostics of technical facilities such as reactors. It enables both early detection of process parameters deviations enabling effective control and detection of hazards resulting in failure. In this context, a higher level of reliability can be achieved by using the developed algorithm.

## References

1. Anders D, Rzasa M. The possibility of composting animal waste products. *Environment Protection Engineering* 2007;33(2):7-15.
2. Arevalo J, González FA, Ramos-Pollán R, Oliveira JL, Guevara Lopez MA. Representation learning for mammography mass lesion classification with convolutional neural networks. *Computer Methods and Programs in Biomedicine* 2016;127: 248-257, <https://doi.org/10.1016/j.cmpb.2015.12.014>.
3. Babout L, Grudziń K, Wiącek J, Niedostatkiwicz M, Karpiński B, Szkodo M. Selection of material for X-ray tomography analysis and DEM simulations: comparison between granular materials of biological and non-biological origins. *Granular Matter* 2018; 20(3): 38, <https://doi.org/10.1007/s10035-018-0809-y>.
4. Banasiak R, Wajman R, Jaworski T, Fiderek P, Fidos H, Nowakowski J, Sankowski D. Study on two-phase flow regime visualization and identification using 3D electrical capacitance tomography and fuzzy-logic classification. *International Journal of Multiphase Flow* 2014; 58: 1-14, <https://doi.org/10.1016/j.ijmultiphaseflow.2013.07.003>.
5. Bartusek K, Fiala P, Mikulka J. Numerical modeling of magnetic field deformation as related to susceptibility measured with an MR system. *Radioengineering* 2008;17(4):113-118.
6. Bishop CM. *Pattern Recognition and Machine Learning*. Springer-Verlag New York 2006.
7. Chen H, Ni D, Qin J, Li S, Yang X, Wang T, Heng PA. Standard Plane Localization in Fetal Ultrasound via Domain Transferred Deep Neural Networks. *IEEE Journal of Biomedical and Health Informatics* 2015; 19(5): 1627-1636, <https://doi.org/10.1109/JBHI.2015.2425041>.

An important achievement of the research is the noise-resistant algorithm based on multiple convolutional neural networks (MCNN), which, despite being trained on simulation data, effectively reconstructs objects hidden inside the tank, regardless of their shape, quantity, location or dimensions, based on real measurements. The factor that allows achieving good tomographic reconstruction is the training of many neural networks with one cluster output instead of one CNN with multiple outputs. Simulation experiments carried out for selected UST cases have shown that the newly developed MCNN method can be successfully used to generate 2D monochrome images based on the ultrasonic wave time-of-flight measurements.

In order to better verify the quality of the resulting solutions, the CNN was compared with five popular classification methods that could be used interchangeably (Table 4). The comparative analysis of the accuracy indicators for CNN, ANN, LSVM, Classification Tree, KNN and Naive Bayes showed that the newly developed algorithmic method of CNN most accurately reconstructs a single cluster of the image.

As a result of the tests, both based on simulation and real data, it can be concluded that the reconstructions correctly reflect the position of the inclusions. Images obtained from real measurements show slightly too large inclusion diameters. Simulation data images do not have this error. The reason for problems in the correct representation of the inclusion shape is the low resolution of the output image (32x32). It is worth noting that the MCNN algorithm is able to equally well image objects located both in the center of the tank and close to its walls. The algorithm also has the advantage of being able to image both single and multiple inclusions. It is worth noting that the obtained imaging efficiency exceeds 95%.

A way to increase the effectiveness of the algorithm could be to combine EIT methods with UST. This requires the installation of both types of sensors around the reactor under test: electrodes for EIT and transducers for UST. This idea requires some technical problems to be resolved to deploy a large number of different sensors in close proximity.

The topic of the research is up to date, which has been appropriately substantiated with reference to the present state of knowledge. Thanks to the conducted research, it was possible to develop a tomographic algorithm, whose high resistance to noise allows for generating detailed images in real conditions. This was confirmed during special tests. The presented results are of key importance for the development of knowledge and innovation in the field of non-invasive applications for monitoring methods of industrial facilities - especially tank reactors. It is planned to continue research towards the development of a hybrid method covering both the physical (EIT + UST) and algorithmic layers.

8. Du X, Li J, Feng H, Chen S. Image reconstruction of internal defects in wood based on segmented propagation rays of stress waves. *Applied Sciences (Switzerland)* 2018; 8(10): 1778, <https://doi.org/10.3390/app8101778>.
9. Goetzke-Pala A, Hoła A, Sadowski Ł. A non-destructive method of the evaluation of the moisture in saline brick walls using artificial neural networks. *Archives of Civil and Mechanical Engineering* 2018; 18(4): 1729-1742, <https://doi.org/10.1016/j.acme.2018.07.004>.
10. Gola A, Kłosowski G. Application of Fuzzy Logic and Genetic Algorithms in Automated Works Transport Organization. In: *Advances in Intelligent Systems and Computing*. Vol 620. Springer, Cham 2018: 29-36, [https://doi.org/10.1007/978-3-319-62410-5\\_4](https://doi.org/10.1007/978-3-319-62410-5_4).
11. Khairi MTM, Ibrahim S, Yunus MAM, Famararzi M, Sean GP, Puspanathan J, Abid A. Ultrasound computed tomography for material inspection: Principles, design and applications. *Measurement* 2019; 146: 490-523, <https://doi.org/10.1016/j.measurement.2019.06.053>.
12. Kłosowski G, Kozłowski E, Gola A. Integer Linear Programming in Optimization of Waste After Cutting in the Furniture Manufacturing. In: Burduk A., Mazurkiewicz D. (Eds) *Intelligent Systems in Production Engineering and Maintenance - ISPEM 2017*, vol 637, 2018: 260-270, [https://doi.org/10.1007/978-3-319-64465-3\\_26](https://doi.org/10.1007/978-3-319-64465-3_26).
13. Kłosowski G, Rymarczyk T, Gola A. Increasing the reliability of flood embankments with neural imaging method. *Applied Sciences* 2018; 8(9): 1457, <https://doi.org/10.3390/app8091457>.
14. Kozłowski E., Mazurkiewicz D., Kowalska B., Kowalski D. – Binary Linear Programming as a Decision-Making Aid for Water Intake Operators. In book: *Intelligent Systems in Production Engineering and Maintenance – ISPEM 2017*, Edition: *Advances in Intelligent Systems and Computing* vol. 637. Publisher: Springer International Publishing, Editors: Anna Burduk, Dariusz Mazurkiewicz, pp.199-208, DOI: 10.1007/978-3-319-64465-3\_20.
15. Krawczyk A, Korzeniewska E. Magnetophosphenes - history and contemporary implications. *Przegląd Elektrotechniczny* 2018; 1(1): 63-66, <https://doi.org/10.15199/48.2018.01.16>.
16. Kryszyn J, Smolik W. Toolbox for 3D modelling and image reconstruction in electrical capacitance tomography. *Informatics Control Measurement in Economy and Environment Protection* 2017; 7(1): 137-145, <https://doi.org/10.5604/01.3001.0010.4603>.
17. Kryszyn J, Wanta DM, Smolik WT. Gain Adjustment for Signal-to-Noise Ratio Improvement in Electrical Capacitance Tomography System EVT4. *IEEE Sensors Journal* 2017; 17(24): 8107-8116, <https://doi.org/10.1109/JSEN.2017.2744985>.
18. Lei J, Liu Q, Wang X. Deep Learning-Based Inversion Method for Imaging Problems in Electrical Capacitance Tomography. *IEEE Transactions on Instrumentation and Measurement* 2018; 67(9): 2107-2118, <https://doi.org/10.1109/TIM.2018.2811228>.
19. Li X, Li J, He D, Qu Y. Gear pitting fault diagnosis using raw acoustic emission signal based on deep learning. *Eksploracja i Niezawodność - Maintenance and Reliability* 2019; 21(3): 403-410, <https://doi.org/10.17531/ein.2019.3.6>.
20. Lopato P, Chady T, Sikora R, Gratkowski S, Ziolkowski M. Full wave numerical modelling of terahertz systems for nondestructive evaluation of dielectric structures. *COMPEL - The international journal for computation and mathematics in electrical and electronic engineering* 2013; 32(3): 736-749, <https://doi.org/10.1108/03321641311305719>.
21. Ma J, Wu F, Zhu J, Xu D, Kong D. A pre-trained convolutional neural network based method for thyroid nodule diagnosis. *Ultrasonics* 2017; 73: 221-230, <https://doi.org/10.1016/j.ultras.2016.09.011>.
22. Majchrowicz M, Kapusta P, Jackowska-Strumiłło L, Sankowski D. Acceleration of image reconstruction process in the electrical capacitance tomography 3D in heterogeneous, multi-GPU system. *Informatics Control Measurement in Economy and Environment Protection* 2017; 7(1): 37-41, <https://doi.org/10.5604/01.3001.0010.4579>.
23. Mikulka J. GPU-Accelerated Reconstruction of T2 Maps in Magnetic Resonance Imaging. *Measurement Science Review* 2015; 15(4): 210-218, <https://doi.org/10.1515/msr-2015-0029>.
24. Podgórní E, Rząsa M. Investigation of the effects of salinity and temperature on the removal of iron from water by aeration, filtration, and coagulation. *Polish Journal of Environmental Studies* 2014; 23(6): 2157-2161, <https://doi.org/10.15244/pjoes/24927>.
25. Psuj G. Multi-Sensor Data Integration Using Deep Learning for Characterization of Defects in Steel Elements. *Sensors* 2018; 18(2): 292, <https://doi.org/10.3390/s18010292>.
26. Qayyum A, Anwar SM, Awais M, Majid M. Medical image retrieval using deep convolutional neural network. *Neurocomputing* 2017; 266: 8-20, <https://doi.org/10.1016/j.neucom.2017.05.025>.
27. Romanowski A. Big Data-Driven Contextual Processing Methods for Electrical Capacitance Tomography. *IEEE Transactions on Industrial Informatics* 2019; 15(3): 1609-1618, <https://doi.org/10.1109/TII.2018.2855200>.
28. Romanowski A. Contextual Processing of Electrical Capacitance Tomography Measurement Data for Temporal Modeling of Pneumatic Conveying Process. In: 2018 Federated Conference on Computer Science and Information Systems (FedCSIS) 2018: 283-286, <https://doi.org/10.15439/2018F171>.
29. Romanowski A, Łuczak P, Grudzień K. X-ray Imaging Analysis of Silo Flow Parameters Based on Trace Particles Using Targeted Crowdsourcing. *Sensors* 2019; 19(15): 3317, <https://doi.org/10.3390/s19153317>.
30. Rymarczyk T. New methods to determine moisture areas by electrical impedance tomography. Kojima F, Kobayashi F, Nakamoto H, eds. *International Journal of Applied Electromagnetics and Mechanics* 2016; 52(1-2): 79-87, <https://doi.org/10.3233/JAE-162071>.
31. Rymarczyk T. Using electrical impedance tomography to monitoring flood banks. In: *International Journal of Applied Electromagnetics and Mechanics* 2014; 45: 489-494, <https://doi.org/10.3233/JAE-141868>.
32. Rymarczyk T, Adamkiewicz P, Duda K, Szumowski J, Sikora J. New electrical tomographic method to determine dampness in historical buildings. *Archives of Electrical Engineering* 2016; 65(2): 273-283, <https://doi.org/10.1515/aee-2016-0019>.
33. Rymarczyk T, Kłosowski G, Cieplak T, Kozłowski E, Kania K. Application of a regressive neural network with autoencoder for monochromatic images in ultrasound tomography. In: *Institute of Electrical and Electronics Engineers (IEEE)* 2019: 156-160, <https://doi.org/10.23919/PTZE.2019.8781750>.
34. Rząsa MR. A new transducer of double processing for capacitive tomography. *Metrology and Measurement Systems* 2007; 14(2): 291-305.
35. Rząsa MR, Dobrowolski B. The prototype capacitance tomography sensor with increased sensitivity near the wall. *Journal of Energy Science* 2010; 1(1):133-145.
36. Sezer A, Basri Sezer H. Convolutional neural network based diagnosis of bone pathologies of proximal humerus. *Neurocomputing* 2019, <https://doi.org/10.1016/j.neucom.2018.11.115>.
37. Shahdoosti HR, Rahemi Z. Edge-preserving image denoising using a deep convolutional neural network. *Signal Processing* 2019; 159: 20-

- 32, <https://doi.org/10.1016/j.sigpro.2019.01.017>.
38. Świdorski A, Józwiak A, Jachimowski R. Operational quality measures of vehicles applied for the transport services evaluation using artificial neural networks. *Eksploracja i Niezawodność - Maintenance and Reliability* 2018; 20(2): 292-299, <https://doi.org/10.17531/ein.2018.2.16>.
39. Szczesny A, Korzeniewska E. Selection of the method for the earthing resistance measurement. *Przegląd Elektrotechniczny* 2018; 94(12): 178-181.
40. Vališ D, Forbelská M, Vintr Z, Hasilová K, Leuchter J. Platinum thermometer failure estimation based on dynamic linear models. *Engineering Failure Analysis* 2019; 101: 418-435, <https://doi.org/10.1016/j.engfailanal.2019.03.024>.
41. Vališ D, Mazurkiewicz D. Application of selected Levy processes for degradation modelling of long range mine belt using real-time data. *Archives of Civil and Mechanical Engineering* 2018; 18(4): 1430-1440, <https://doi.org/10.1016/j.acme.2018.05.006>.
42. Wajman R, Fiderek P, Fidos H, Jaworski T, Nowakowski J, Sankowski D, Banasiak R. Metrological evaluation of a 3D electrical capacitance tomography measurement system for two-phase flow fraction determination. *Measurement Science and Technology* 2013; 24(6): 065302, <https://doi.org/10.1088/0957-0233/24/6/065302>.
43. Zhang Q, Xiao Y, Dai W, Suo J, Wang C, Shi J, Zheng H. Deep learning based classification of breast tumors with shear-wave elastography. *Ultrasonics* 2016; 72: 150-157, <https://doi.org/10.1016/j.ultras.2016.08.004>.
44. Zhao R, Yan R, Chen Z, Mao K, Wang P, Gao RX. Deep learning and its applications to machine health monitoring. *Mechanical Systems and Signal Processing* 2019; 115: 213-237, <https://doi.org/10.1016/j.ymsp.2018.05.050>.
45. Ziolkowski M, Gratkowski S, Zywicka AR. Analytical and numerical models of the magnetoacoustic tomography with magnetic induction. *COMPEL - The International Journal for Computation and Mathematics in Electrical and Electronic Engineering* 2018; 37(2): 538-548, <https://doi.org/10.1108/COMPEL-12-2016-0530>.

---

**Grzegorz KŁOSOWSKI**

Lublin University of Technology  
Department of Organization of Enterprise  
ul. Nadbystrzycka 38D, 20-618 Lublin, Poland

**Tomasz RYMARCZYK****Konrad KANIA**

University of Economics and Innovation  
ul. Projektowa 4, 20-209 Lublin, Poland  
Research and Development Center, Netrix S.A.  
ul. Związkowa 26, 20-148 Lublin, Poland

**Antoni ŚWIĆ**

Lublin University of Technology  
Institute of Technological Systems of Information  
ul. Nadbystrzycka 38D, 20-618 Lublin, Poland

**Tomasz CIEPLAK**

Lublin University of Technology  
Department of Organization of Enterprise  
ul. Nadbystrzycka 38D, 20-618 Lublin, Poland

E-mails: [g.klosowski@pollub.pl](mailto:g.klosowski@pollub.pl), [tomasz@rymarczyk.com](mailto:tomasz@rymarczyk.com),  
[konrad.kania@netrix.com.pl](mailto:konrad.kania@netrix.com.pl), [a.swic@pollub.pl](mailto:a.swic@pollub.pl), [t.cieplak@pollub.pl](mailto:t.cieplak@pollub.pl)

---